Science and Technology of Advanced Materials 3 (2002) 327–334

Thermal shock and thermal fatigue study of ceramic materials on a newly developed ascending thermal shock test equipment

P.K. Panda[a,*], T.S. Kannan[a], J. Dubois[b], C. Olagnon[b], G. Fantozzi[b]

[a]*Materials Science Division, National Aerospace Laboratories, Bangalore, 560017, India*
[b]*GEMPPM, INSA de LYON, 69621 Villeurbanne Cedex, France*

Received 24 April 2001; revised 11 May 2002; accepted 2 July 2002

Abstract

A test equipment was designed to study thermal shock and thermal fatigue of ceramic materials subjected to fast heating (ascending). The equipment was designed to generate thermal stress in a test specimen by heating one surface of it by an oxy-hydrogen flame while cooling the opposite surface. The sample cracked when thermal stress exceeded its mechanical strength. The in situ crack formation was detected by an acoustic emission system coupled to the set up. The hot zone temperature was measured by an infra red pyrometer. The equipment was also designed to run thermal fatigue test cycles in automatic mode between two selected temperatures. The temperature and thermal stress distribution in the test specimen were modelled using finite element software. The effect of temperature distribution of the top and bottom surfaces on thermal stresses was studied. It was observed that the thermal stress is very sensitive to the temperature distribution on the top surface and maximum near the periphery of the top surface. This was in agreement with the experimental results in which the cracks were originated from the periphery of top surface. It was also observed that the failure temperature was higher for thicker samples.

Keywords: Thermal shock; Thermal fatigue; Test equipment; Modelling; Finite element

1. Introduction

Ceramic materials are widely used as structural members in high temperature applications, e.g. as refractories, as heat engine components, as dies in metal forming industries, as radomes, as catalytic ignitors in aero-engines, etc. due to their high melting points and good mechanical strength at high temperatures. These materials fail when subjected to a sudden change in temperature (thermal shock) or on repeated cycling between two temperatures (thermal fatigue). The sudden change in the surrounding temperature generates temperature gradient, thereby, the ceramic body experiences thermal stress. The failure occurs when the thermal stress exceeds the strength of the material in that mode of stressing. For example, when a ceramic material is heated suddenly from room temperature, the surface of the material attains high temperature in a very short time. The surface expands and experiences compressive stress. However, the interior of the sample still remains at low temperature (due to low thermal conductivity) and expands less than the surface. Therefore, the interior experiences tensile stress. In contrast, on cooling, the surface experiences tensile stress while the interior experiences compressive stress. During the process of fast heating or cooling, the temperature differences and thermal stresses change with time rapidly (transient state) before they reach a constant difference (steady state).

The thermal stress experienced by a material depends on rate of heating or cooling apart from its own thermo-mechanical properties. Therefore, it is appropriate to test these materials for thermal shock or thermal fatigue resistance under simulated conditions before actual use. There are many test methods available for measurement of thermal shock resistance of ceramic materials. They can be broadly classified into two groups: (1) thermal shock during heating (ascendant) and (2) thermal shock during cooling (descendant). Some known examples of ascending thermal shock tests are: hot-gas jet method [1], high power radiation [2], melt immersion test [3], ribbon test method [4], high power laser heating method [5], etc. Similarly, some known

* Corresponding author. Address: Materials Science Division, National Aerospace Laboratories, Bangalore 17, 560017, India. Tel.: +91-80-508-6146.
E-mail address: pkpanda@css.cmmacs.ernet.in (P.K. Panda).

1468-6996/02/$ - see front matter
PII: S1468-6996(02)00029-3

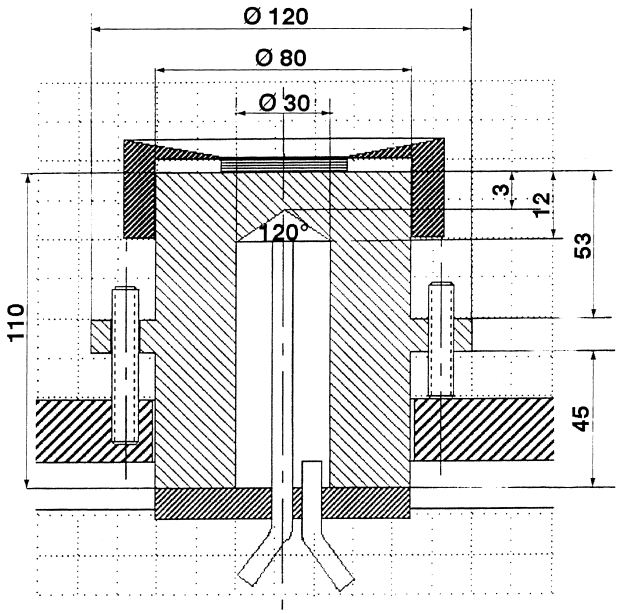

Fig. 1. Drawing of sample holder with water cooling facility (all dimensions in mm).

test methods for descendant thermal shock are by: quenching in water [6], fluidised beds [7] or a cold-air jet impinging on hot discs [8,9], quenching in contact with huge brass rods [10] and indentation method [11]. The thermal fatigue test methods include: the quench method [12], repetitive-heating method [13], etc. However, the most popular thermal shock test method is the water quench method in which samples are heated to a particular temperature and than quenched in water bath. The residual strength after the quench and the critical temperature difference (ΔT_c) are the two parameters used to grade the thermal shock resistance of various materials. However, water quench experiment generates higher rates of heat transfer than a material would experience during its actual use. Therefore, the material fails relatively at a lower critical temperature difference. In addition, heat transfer coefficient involved in a water quench method is difficult to measure due to vaporisation of water, thereby, making modelling of thermal shock experiment difficult. Moreover, this method is of little relevance for ceramic materials used in aerospace, as engine components, radomes where thermal shock occurs mostly during heating. Among ascending thermal shock tests, except for laser heating method, which is costly, it is difficult to generate high temperatures suitable for thermal shock test of high strength materials (e.g. silicon nitride, silicon carbide, composites, etc).

This paper deals with the development and standardisation of a test equipment suitable to generate high thermal stress with well defined thermal boundary conditions which allows the study of temperature and thermal stress distribution to study the failure of the material in a simulated condition.

2. Description of the test equipment

The equipment is designed to create a temperature gradient in a test sample by heating one side of it while cooling the opposite side by keeping it in contact with a water-cooled copper block. The thermal stress created due to the temperature gradient is given by,

$$\sigma = \frac{E\alpha\Delta T}{1-\nu}$$

where σ is the thermal stress, α, the coefficient of thermal expansion, ΔT, the temperature gradient, and ν, the Poisson's ratio.

The test equipment comprises of the following parts: (1) sample holder (2) heat generation system (3) temperature measurement system (4) crack detection system (5) microprocessor based automation system and (6) data acquisition system.

2.1. Sample holder

The sample holder is in the form of a cylindrical copper block of 80 mm diameter and 110 mm long (Fig. 1). It is internally cut out to enable the circulating cold water to reach very near to the top surface of the copper block (for efficient cooling). The water flow rate is measured by a flow meter and is in the range of 0.15–5.0 l/min.

2.2. Heat generation system

The heat generation system consists of an oxy-hydrogen torch that heats the sample. Initially, oxy-acetylene combination was tried. It was noticed that the measurement of hot temperature was interfered by CO_2 and soot particles generated during combustion of fuel gas. Hence, an oxy-hydrogen flame was used to avoid the interference. The oxy-hydrogen torch is fixed to a vertical stand that can be moved vertically to adjust the distance between the nozzle tip and the sample surface. The torch can also be moved horizontally to focus the flame at the centre of the sample. An electric spark generated by passing a high voltage between two brass rod tips ignites the flame automatically. The heating rate is controlled by varying the oxy-hydrogen gas mixture and by varying the distance of nozzle tips from the sample surface. Different nozzles (80–400 number, the number indicates the flow rate of gas in litres at normal temperature and pressure) were used to vary the size of the hot zone. The oxy-hydrogen gas flow rates are regulated/measured by flow meters. For safety purpose, an ultra violet flame detector is provided very near to the flame. By the above method, a sample can be heated up to 2000 °C in a short time of $\leq$20 s.

2.3. Temperature measurement system

The temperature measurement system consists of an infra

red pyrometer to measure the temperature of the hot zone and a thermocouple to measure the temperature at the periphery of the sample. The temperature of the central hot zone of the sample is measured by an infra red mono-colour pyrometer (Model-IRCON Modline plus, series 7000, special 200/2000 °C from M/s IRCON Inc., USA) by focussing the zone of detection (field of view) of IR pyrometer inside the hot zone. The pyrometer is fixed to an adjustable stand, which in turn is fixed to top of the table. The axis of the pyrometer makes an angle of 75° to the sample surface. The temperatures at different distances from the centre of the sample are measured by moving the 'field of view' across the diameter of the sample. The periphery temperature is measured by using an ultra sensitive chromel–alumel (type K) thermocouple wires (0.25 mm diameter). The wire passes through the circular waveguide cover and a perfect contact between the thermocouple tip and the sample is ensured by a spring loading mechanism. The temperatures measured by IR pyrometer and thermocouple are acquired in real time via the two parametric parallel ports available in the acoustic emission (AE) monitoring system and stored simultaneously in a PC.

2.4. Crack detection system

The failure of the test sample during thermal shock/thermal fatigue test is detected by an AE detector system (PAC-BUS model 3100 of Euro Physical Acoustics Inc., France). It consists of a PZT-5 (R30) sensor, a wave-guide, a filter and an amplifier. The cylindrical shaped wave-guide made out of stainless steel with a central hole and is placed over the test sample but without touching the copper block. Therefore, the flame heating is restricted to the cutout area. The sensor is attached to the wave-guide by a suitable couplant (usually silicone grease). The acoustic signals generated during failure (cracking) of the sample are picked up by the sensor through the wave-guide. The signals are stored in a PC after noise filtration and amplification.

2.5. Automation system

The equipment is designed to run thermal fatigue cycles by a microprocessor controller in a programmable mode. The fatigue tests require repeated thermal shock heating of sample to the same maximum temperature followed by cooling. The failure tests are conducted by feeding the maximum temperature of heating, heating time, cooling time, number of cycles to perform, etc. The test is run in automatic mode till specified numbers of cycles are completed or till the failure of the sample (detected by AE) whichever is earlier.

2.6. Data acquisition system

The data acquisition system consists of AE set up along with a PC. The AE set up collects the AE data as well as the temperature data collected by the pyrometer and the thermocouple and are simultaneously stored or displayed in real time on the screen.

3. Experimental procedures

3.1. Thermal shock test

A circular disc shaped test specimen of 30 mm diameter and 3–5 mm thick is fixed at the centre of the copper block with a conducting paste of fine metal powder (e.g. aluminium metal) for good contact and efficient cooling. The centre of the top surface of the sample is marked to focus the pyrometer for temperature measurement. Various heating parameters such as oxygen to hydrogen gas flow ratio, the distance between the nozzle tip and the sample surface, nozzle number, water cooling rates, etc. are chosen depending upon the thermal stress resistance of material. The IR pyrometer is focussed at the centre of the test specimen. The AE sensor and thermocouple are properly fixed on to the circular wave-guide and the sample. The test is run and temperatures (hot and periphery) and AE data generated during the test are saved in a file. A typical real time temperature and AE profile recorded during thermal shock test of Si_3N_4 is presented in Fig. 2.

3.2. Thermal fatigue test

The thermal fatigue test is typically carried out at a temperature below the maximum temperature at which the sample cracks. Initially, oxy-hydrogen gas mixture is selected suitably to get the required maximum temperature. Thermal fatigue test of an alumina test specimen was carried out at 400 °C with heating and cooling time fixed for 15 and 20 s, respectively. Typical temperature cycles employed during thermal fatigue test are presented in Fig. 3 and the AEs resulted after 50, 100, 150 and 200 cycles are presented in Fig. 4. It could be seen that the continuous AE signals occurred at higher cycles while no AE signal was present at the beginning of the test. The continuous AE signals generated are attributed to micro-cracking phenomena. The sample was also observed under microscope after dye test in which a number of pitting holes was observed.

4. Modelling

4.1. Meshing

Because of axial symmetry of the sample, a two-dimensional axis-symmetric plane of the sample was considered for modelling. The plane was meshed with rectangular elements (171 elements).

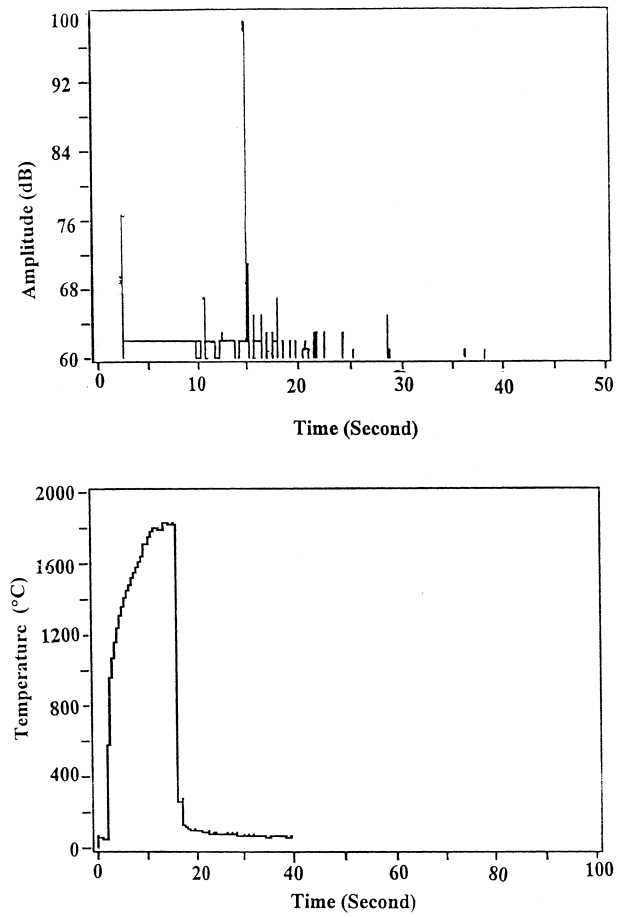

Fig. 2. The temperature (bottom) and AE amplitude (top) recorded during thermal shock test of silicon nitride sample.

4.2. Boundary conditions

For modelling of temperature and thermal stress distribution in the test, it is necessary to apply thermal boundary conditions in finite element (FE) software either in the form of heat transfer coefficient or in the form of temperature values at different grid points. Due to simplicity, the temperature distribution on hot face of the sample was used as thermal boundary. The temperature of the hot zone was measured during failure of the sample. The temperature values at other places in radial direction were measured by extrapolating proportionately from the previously measured temperatures corresponding to central temperatures less than critical temperature difference. The extrapolation is necessary because it is not possible to record temperature values at other points once the sample cracks. The extrapolation method used to generate temperature values are presented as follows.

4.3. Temperature measurement by extrapolation method

To generate the temperature profiles, the oxy-hydrogen flow was maintained same. The temperature at the central point was recorded for 20 s, the flame was then put off. The pyrometer was shifted 1 mm horizontally so as to measure the temperature 1 mm away from the centre. This was repeated for 10 points to generate temperature profiles up to 10 mm away from the centre of the sample. This completed one trial. The oxygen to hydrogen gas ratio was changed suitably to generate higher temperature but was maintained below its critical temperature. The temperature profiles were recorded by repeating the procedure followed in trial one. Finally, a fresh sample was heated to the critical temperature where it cracked. The temperature values at different radial distances from centre corresponding to the cracking temperature of the sample (at the centre) were computed by method of proportionate increments of temperature for each radial distance of 1 mm as per the formula given below.

$$\frac{T3(0) - T2(0)}{T2(0) - T1(0)} = \frac{T3(1) - T2(1)}{T2(1) - T1(1)}$$

where $T3(0)$ is the temperature at the centre of the sample

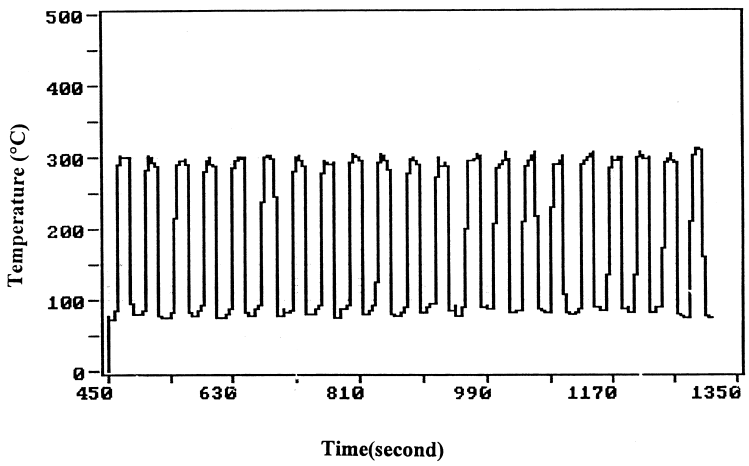

Fig. 3. Typical temperature cycles employed for thermal fatigue test of alumina.

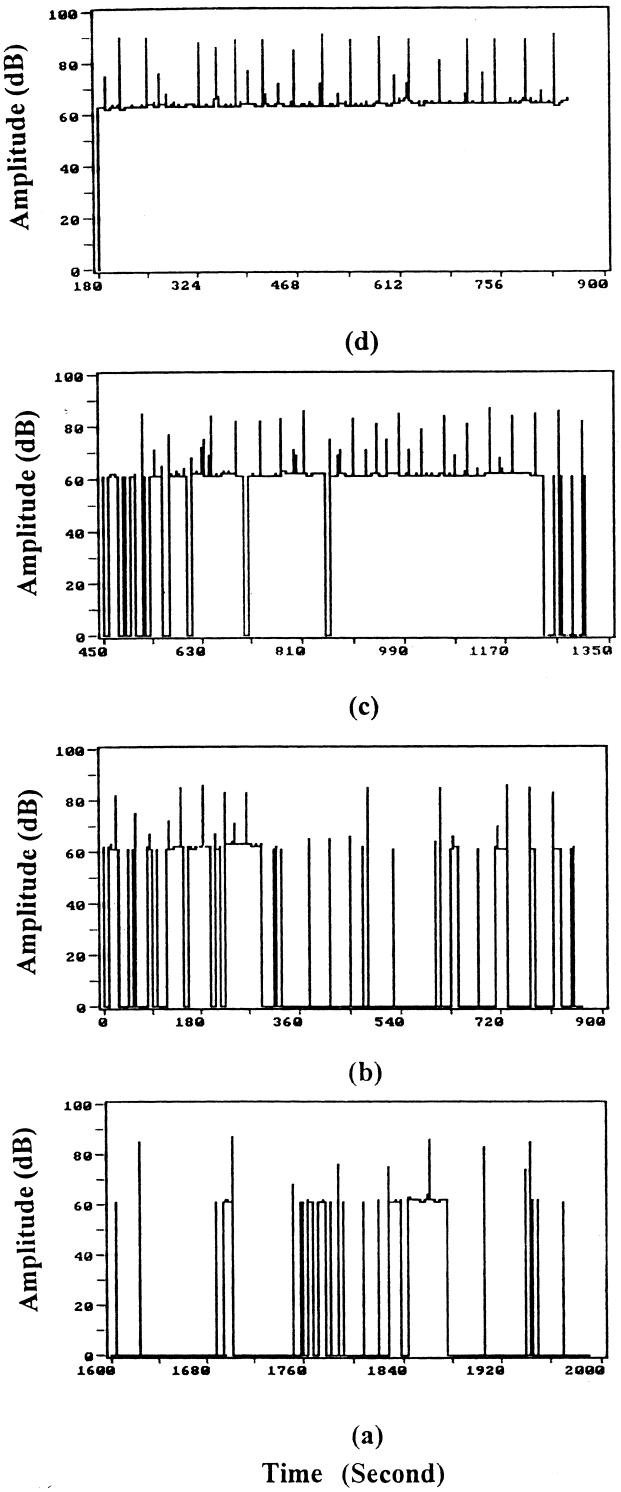

Fig. 4. Typical AE data generated during thermal fatigue cycles of alumina after (a) 50 cycles, (b) 100 cycles, (c) 150 cycles, (d) 200 cycles of heating and cooling.

measured by the pyrometer at the time of cracking due to thermal shock; $T2(0)$ and $T1(0)$ are the temperatures at the centre of the sample measured by the pyrometer in Trial 2 and Trial 1, respectively; $T2(1)$ and $T1(1)$ are the temperatures at 1 mm radial distance from the centre of

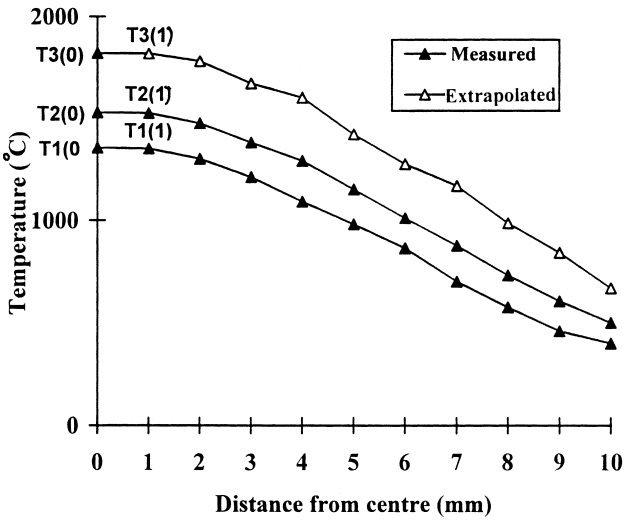

Fig. 5. Temperatures measured and extrapolated at different distances from the centre of the test specimen.

the sample measured by pyrometer in Trial 2 and Trial 1, respectively; and $T3(1)$ is the extrapolated temperature at 1 mm away from the centre.

The measured and extrapolated temperature values at different radial distances from centre are presented in Fig. 5 These extrapolated temperature values vary with the time till they reach the maximum temperature and these were applied as thermal boundary condition for each corresponding grid value for FE modelling. A typical axis-symmetric plane with thermal boundary used for modelling is presented in Fig. 6.

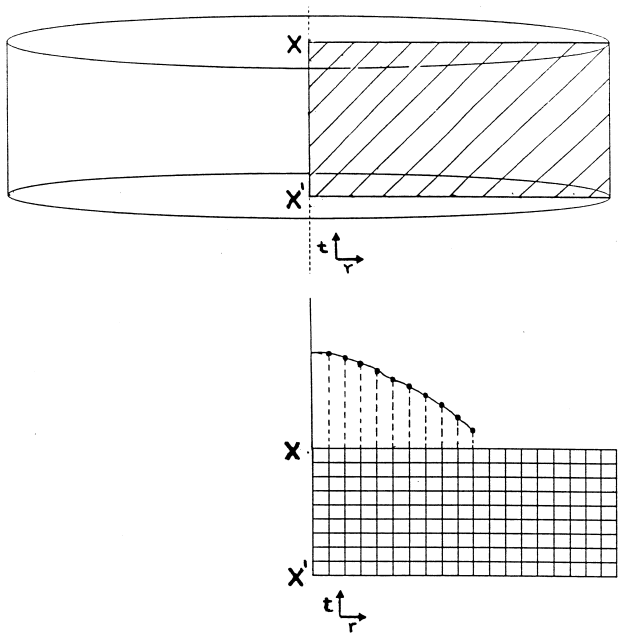

Fig. 6. Finite element model of an axis-symmetric plane of the sample with rectangular elements and the temperature profile applied on the hot surface. (T is temperature, r is distance from the centre, t is thickness direction).

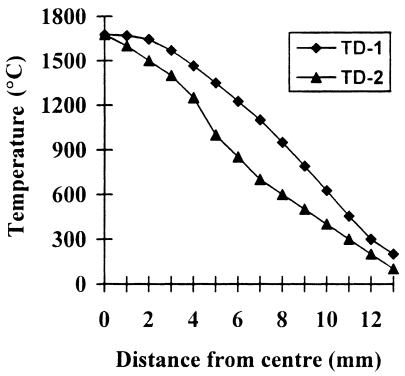

Fig. 7. Typical temperature distributions used for thermal stress calculations.

5. Results and discussion

5.1. Effect of temperature distribution on hot face

Two different types of temperature profiles (i) one with gradual temperature drop (TD-1) and (ii) with relatively sharp temperature drop (TD-2) were used to find their effects on thermal stress. TD-1 was actually recorded by the pyrometer during heating on a Si_3N_4 test specimen while TD-2 was generated from TD-1 by decreasing the temperature values of TD-1 at all grid points except the central grid point. The temperature distribution used for modelling is presented in Fig. 7. The thermo-mechanical properties of Si_3N_4 used for modelling are presented in Table 1. For thermal stress modelling, the co-ordinates of the grid points of the central axis ($X = 0$) were treated as fixed points.

The maximum tensile stress was 544 MPa for TD-1 and 430 MPa for TD-2. The thermal stress was 1050 MPa when all the grid points were 1676 °C on the top surface corresponding to the condition of constant heat flux. From the above, it could be concluded that the thermal stress is the maximum when all the grid points are at high temperatures and thermal stress decreases with higher temperature gradients on top surface.

5.2. Effect of temperature distribution on cold face

The effect of bottom temperature on thermal stress was studied by assuming two temperatures, 200 and 30 °C while the top surface temperature was maintained at 1676 °C. It was found that the thermal stress was 1057 MPa for 30 °C while it was 1051 MPa for 200 °C. This concludes that thermal stress is not very sensitive to the change in base temperature. Therefore, accurate temperature measurement of the bottom surface of the sample is not critical. It could also be concluded that the critical temperature difference (ΔT_c), the difference in maximum hot temperature and bottom surface temperature is no more characteristics of the equipment since the thermal stress is independent of cold face temperature. However, the temperature of the hot spot (T_{max}) can be considered as the characteristic temperature for the failure of the material.

Table 1
Thermo-mechanical parameters of Si_3N_4 used for modelling

Thermo-mechanical properties	Units	Test sample
Density (ρ)	kg/m^3	3100
Thermal conductivity (K)	W/m °C	13
Coefficient of thermal expansion (α)	°C^{-1}	3.3×10^{-6}
Young's modulus (E)	GPa	300
Heat capacity (C_P)	J/kg °C	1200
Poisson's ratio (ν)	–	0.3

5.3. Effect of thermal conductivity of interface

The test sample is generally fixed to copper block by a suitable adhesive. Obviously, the thermal conductivity of the adhesive would play significant role in temperature and thermal stress in the sample. To find the effect of thermal conductivity of this adhesive, three different thermal conductivity values of the interface (0.2, 20, 200 W/m K) were used for modelling. The values were selected corresponding to the conductivity values of high vacuum grease (0.2 W/m K) used initially to fix the sample to the copper block and that of metal paste (200 W/m K) corresponding to the conductivity of Al metal used as interface. From modelling studies, the temperature values at the centre of the bottom face were found to be 967.7, 119.0 and 57.95 °C corresponding to interface conductivity values of 0.2, 20 and 200 W/m K. The maximum temperatures at the top periphery of the sample were found to be of 120.1, 67.0 and 57.71 °C, respectively. The corresponding thermal stress values were found to be 555.1, 546.5 and 550.8 MPa, respectively. Therefore, it is concluded that the thermal conductivity of the interface does not affect the maximum thermal stress significantly but it changes the temperature distribution in the sample. The temperature at the bottom face increases with a decrease in thermal conductivity of the interface. This is because of the low thermal conductivity of the interface, which prevented heat loss, and the heat was utilised to increase the temperature of the sample. The thermal stress was not affected significantly by interface conductivity. This could be attributed to the localised heating at the centre of the specimen. The temperature drop over a small-localised volume surrounding the central hot region was very high compared to the temperature variation near bottom face. Hence, thermal stress was mainly influenced by the temperature distribution on the top surface and was not affected by the temperature distribution at the bottom surface. Therefore, accurate measurement of temperature of the bottom face is not very critical for thermal stress calculation.

It is ideal to have bottom face temperature very close to the room temperature so that the bottom face temperature

Table 2
Failure temperature (T_f) for alumina of different thickness during thermal shock test

Thickness of the sample (mm)	Failure temperature (°C)	Calculated thermal stress (MPa)
2	342 ± 33	125.9
3	390 ± 39	138.1
4	557 ± 75	178.1
5	647 ± 100	197.0
6	700 ± 60	198.0

could be taken approximately as that of water cooling temperature/room temperature for modelling. This could also avoid the temperature measurement at the interface, which is very difficult to place a thermocouple to measure accurate temperature. Hence, low conductivity vacuum grease was replaced by high conductivity paste of Al metal.

5.4. Maximum stressed zone (origin of cracks)

To find the origin of cracks and hence the region of maximum thermal stress, polished alumina samples were indented (i) near the periphery of the top surface (~2 mm away from the periphery) (ii) at the centre of the bottom face and (iii) both near periphery and at the centre. Three samples were used for each test and a load of 50 N was used for indentation. The samples were then subjected to thermal shock test. It was found that the cracks passed through the indents except in the centre of one sample where it was indented at the centre as well as near periphery. This concludes the cracks originate near the periphery because, if it had originated from centre, it would not have necessarily propagated in the direction of the periphery. This observation was confirmed by modelling.

5.5. Effect of thickness of the sample on failure temperature

To find the effect of thickness on critical temperature difference (ΔT_c), alumina samples of 30 mm diameter and thickness in the range of 2–6 mm were subjected to thermal shock test. For reliability of the data, three samples of each thickness were tested. The temperature at which the samples failed (T_f) was presented in Table 2.

From the above results, it was observed that the failure temperature increases with sample thickness. It has been observed for quench experiments that ΔT_c is more for thinner samples. Sherman et al. [14] explained this phenomena due to the increase in compressive stress on the surface with decrease in sample thickness, therefore, the overall tensile stress decreases on the quench surface. Since, the thermal shock due to heating is just opposite to that due to cooling, extending Sherman's explanation, compressive stress should be lower for thinner samples and higher for thicker samples. Therefore, the overall tensile stress should decrease with the increase in sample thickness requiring higher temperature for initiation of failure. The same has been observed from our modelling studies, i.e. that thicker samples need higher ΔT_c compared to thinner samples to generate the same tensile stress level. For example, it could be seen from Table 2 that the temperature values of 700 and 647 °C are required to develop a tensile stress of 197 MPa at the periphery of the sample for 6 and 5 mm thick samples, respectively. Therefore, thicker samples fail at higher temperatures than the thinner samples.

6. Conclusions

The novel thermal shock-cum-thermal fatigue test unit developed is suitable to study the thermal shock and thermal fatigue behaviour of advanced ceramic materials due to sudden heating. The equipment allows simulating thermal shock conditions that prevails in the actual service conditions. It could be concluded that the thermal stress depends mainly on the temperature distribution of the hot face. The thermal stress is also sensitive to thickness of the sample; therefore, samples of same thickness need to be tested to get meaningful results. The degradation in thermo-mechanical properties of materials can be studied well by monitoring AEs generated during thermal fatigue tests.

Acknowledgements

The authors gratefully acknowledge the help and assistance given by A. Cheluvaraju, V.A. Jaleel of NAL and G. Masal, J. Ferreira and H. Kalanthar of INSA de Lyon during the course of this study. The authors thank the Indo-French Centre for Promotion of Advanced Studies (IFCPAR) for financial support.

References

[1] G.C. Wei, J. Walsh, Hot-gas-jet method and apparatus for thermal-shock testing, J. Am. Ceram. Soc. 72 (5) (1989) 286–289.
[2] G.A. Schneider, G. Petzow, Thermal shock testing of ceramics—a new testing method, Am. Ceram. Soc. 74 (1) (1991) 98–102.
[3] W. Dienst, W.H. Scholz, H. Zimmermann, Thermal shock resistance of ceramic materials in melt immersion tests, J. Eu. Ceram. Soc. (5) (1989) 365.
[4] C.E. Semler, T.H. Hawisher, Evaluation of the thermal shock resistance of refractories using the ribbon test method, Am. Ceram. Soc. Bull. 59 (7) (1980) 732–737.
[5] S.G. Schwille, R.A. Tanzili, S. Musikant, Thermal stress testing of advanced optical ceramics by a laser technique, in: D.P.H. Hasselman, R.A. Heller (Eds.), Thermal Stress in Severe Environments, Plenum Press, New York, 1980, pp. 553–566.
[6] D. Lewis III, Thermal shock and thermal shock fatigue testing of ceramics with the water quench test, in: C. Bradt, A.G. Evans, D.P.H. Hasselman, F.F. Lange (Eds.), Fracture Mechanics of Ceramics, vol. 6, Plenum Press, New York, 1983, pp. 487–496.
[7] M. Oguma, C.J. Fairbanks, D.P.H. Hasselman, Thermal stress fracture

of brittle ceramics by conductive heat transfer in a liquid metal quenching medium, J. Am. Ceram. Soc. 69 (4) (1986) C-87–C-88.
[8] K.T. Faber, M.D. Huang, A.G. Evan, Quantitative studies of thermal shock in ceramics based on a novel test technique, J. Am. Ceram. Soc. 64 (5) (1989) 296–301.
[9] J.R. Brokenbrough, L.E. Forsythe, R.L. Rolf, Reliability of brittle materials in thermal shock, J. Am. Ceram. Soc. 69 (8) (1986) 634–637.
[10] W.P. Roger, A.F. Emery, Contact thermal shock test of ceramics, J. Mater. Sci. (1992) 146–152.
[11] T. Anderson, D.J. Rowcliffe, Indentation thermal shock test for ceramics, J. Am. Ceram. Soc. 79 (6) (1996) 1509–1514.
[12] J. Lamon, A method for evaluating the thermal fatigue resistance of ceramics and its application to a fibre reinforced refractory material, J. Mater. Sci. (16) (1981) 2119–2129.
[13] J. Lamon, D. Pherson, Thermal stress failure of ceramics under repeated rapid heatings, J. Am. Ceram. Soc. 74 (6) (1991) 1184–1186.
[14] D. Sherman, D. Schlumm, Thickness effect in thermal shock of alumina ceramics, Script. Mater. 42 (8) (2000) 819–825.